

Claremont Colleges

Scholarship @ Claremont

CMC Senior Theses

CMC Student Scholarship

2019

Giardia lamblia growth in viscoelastic fluids

Kelly Watanabe

Follow this and additional works at: https://scholarship.claremont.edu/cmc_theses



Part of the [Biophysics Commons](#), [Cell Biology Commons](#), [Fluid Dynamics Commons](#), [Parasitic Diseases Commons](#), and the [Statistical, Nonlinear, and Soft Matter Physics Commons](#)

This Open Access Senior Thesis is brought to you by Scholarship@Claremont. It has been accepted for inclusion in this collection by an authorized administrator. For more information, please contact scholarship@cuc.claremont.edu.

Giardia lamblia growth in viscoelastic fluids

A Thesis Presented by

Kelly Watanabe

In Collaboration with Georgetown University,

Department of Physics and

Institute for Soft Matter Synthesis and Metrology and

Department of Biology

To the Keck Science Department

Of Claremont McKenna, Pitzer, and Scripps Colleges

In partial fulfillment of

The degree of Bachelor of Arts in Biophysics

Senior Thesis in Physics

December 9, 2019

Table of Contents

Abstract.....	3
1. Introduction	4
2. Historical Background	4
2.1 <i>Giardia</i> infection.....	4
2.2 <i>Giardia</i> lifecycle.....	4
2.2 Intestinal mucus biology	5
2.3 Mucus variability	6
2.4 Characterization of viscoelastic properties.....	7
2.5 Rheological measurements of mucus	9
2.6 Hydrodynamic model of <i>Giardia</i> attachment	10
2.7 Long Chain Polyacrylamide (LCPAM) in media	12
2.8 LCPAM sonication.....	12
3. Methods.....	14
3.1 Preparing solutions of LCPAM in media.....	14
3.2 Sonicating solutions	14
3.3 Measuring solution rheology	15
3.4 Culturing <i>Giardia</i> for growth curves	16
3.4.1 Cell seeding.....	16
3.4.2 Media refreshing	17
3.4.3 Qualitative growth curves	18
3.4.4 Counting <i>Giardia</i> cells.....	18
3.4.5 Quantitative growth curves.....	19
4. Results.....	20
4.1 Rheology of LCPAM solutions	20
4.2 LCPAM sonication rheology	22
4.3 <i>Giardia</i> growth curves.....	23
4.3.1 Control cells	23
4.3.2 0.4% LCPAM-conditioned cells.....	24
4.3.3 Control cells vs. 0.4% LCPAM-conditioned cells.....	24

5. Discussion.....	26
5.1 LCPAM in water vs. media.....	26
5.2 0.2% vs. 0.4% LCPAM in media	27
5.3 0.4% LCPAM vs intestinal mucus.....	28
5.4 LCPAM rheology variability	29
5.5 LCPAM sonication.....	30
5.6 Adaptation vs. acclimation.....	31
5.7 Future studies.....	33
6. Conclusion.....	34
Acknowledgements.....	35
Literature Cited	36
Supplemental Information.....	42
SI.1 Rheology and qualitative growth curves for Ficoll in media	42
SI.2 Image processing for automated <i>Giardia</i> counting	44

Abstract

Giardia lamblia is a single-celled protozoan parasite that when ingested, causes diarrheal disease and infects 33% of people in developing countries. Previous studies observe *Giardia* in water-like fluids, but *Giardia*'s infectious environment consists of viscoelastic mucus in the small intestine. Therefore, *Giardia* was cultured in viscoelastic fluids, and its population growth was observed *in vitro*. To create shear-thinning viscoelastic fluids, 0.2% and 0.4% long-chain polyacrylamide (LCPAM) was added to cell culture media. *Giardia* was cultured in control media, 0.2% LCPAM, and 0.4% LCPAM, and population growth was quantitatively determined over time. Increasing LCPAM concentration resulted in a solution with higher viscosity and elasticity. Experimental results suggest that *Giardia* growth is delayed in more viscoelastic fluids, but the population adjusts to the viscoelastic environments over time.

1. Introduction

Giardia is a parasite that infects the small intestine of humans and other animals. Although *Giardia* is a major public health concern, the disease mechanisms are still poorly understood. Current knowledge of *Giardia* derives from previous studies of *Giardia's* behavior in water-like fluids. However, *Giardia's* native infectious environment is comprised of intestinal mucus which has different physical properties (viscoelasticity) than water. Therefore, this study aims to (1) compare the rheological characteristics of long-chain polyacrylamide (LCPAM) in *Giardia* culture media with that of intestinal mucus and (2) characterize *Giardia* population growth behavior over time in viscoelastic LCPAM solutions.

2. Historical Background

2.1 Giardia infection. *Giardia lamblia*, also known as *Giardia intestinalis* or *Giardia duodenalis*, is a single-celled protozoan parasite that causes the diarrheal illness giardiasis. When ingested via water contaminated by feces, *Giardia* infects the small intestine. The infectious dose is low; it takes only 10 *Giardia* cysts for a host to become infected¹. In the United States, giardiasis is the most common intestinal parasitic disease for humans², and it infects 33% of people in developing countries³. The incubation period, or time between pathogen exposure and the onset of clinical symptoms, of giardiasis is 1-3 weeks¹.

2.2 Giardia lifecycle. *Giardia* has two life cycle stages: a dormant cyst stage and an active trophozoite stage. Cysts are hardy, resistant forms that can survive in feces and cold water. They are oval-shaped cells that are non-motile and lack flagella. During transmission, the host ingests *Giardia* in the cyst form. *Giardia* undergoes excystation upon passage through

the small intestine. Stomach acids and digestive enzymes activate excystation in which cysts develop into infectious trophozoites⁴. Trophozoites induce epithelial cell apoptosis, which disrupts tight junctions and increases epithelial permeability to pathogens⁵. Flagellated trophozoites colonize the small intestine and reproduce via longitudinal binary fission every 9-12 hours². As trophozoites pass through the colon, encystation occurs in which *Giardia* exits the body as cysts in feces⁶.

2.2 Intestinal mucus biology. The mucus of the small intestine is the physiological environment for disease-causing *Giardia* trophozoites. *Giardia* is a noninvasive parasite, and thus it does not physically penetrate the host tissue. Instead, trophozoites attach to the mucous surface of the intestinal wall.

Gastrointestinal mucus is composed of two layers: a loosely adherent layer and a firmly adherent layer (Figure 1b). The loosely adherent layer resides between the lumen and the firmly adherent layer, and the firmly adherent layer attaches on top of the epithelial cells (Figure 1a). Microorganisms commonly penetrate the loosely adherent layer, but the firmly adherent layer is mostly

nonpenetrable⁷. Intestinal mucous layers are composed of MUC2 mucins which form a mesh-like network (Figure 1b). MUC2 is secreted from the epithelial cells, and the

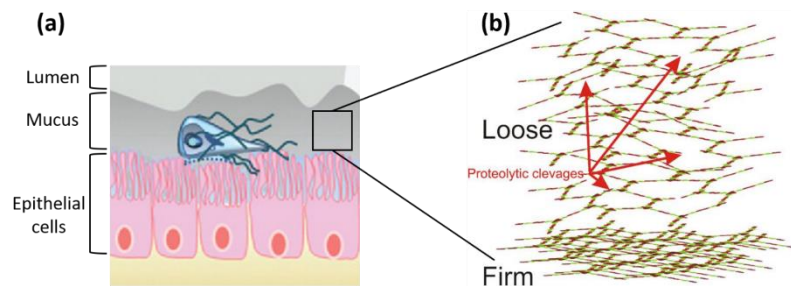


Figure 1. Schematic of intestinal mucus structure. **(a)** *Giardia* transverse the lumen to reside in the mucosal surface and attach to epithelial cells of the intestinal wall⁸. **(b)** The firmly adherent and loosely adherent layers of mucus⁷. The firmly adherent layer has a dense MUC2 network while the loosely adherent layer is more flexible and expanded in volume due to proteolytic cleavages.

firmly adherent layer has a highly structured, densely packed network due to its proximity to the epithelial cells. The firmly adherent layer is freshly secreted and unmodified by enzymes in the lumen. In contrast, the loosely adherent layer is closer to the lumen which contains proteases that cause proteolytic cleavages of the peptide backbone. Since the MUC2 network is stabilized by disulfide bonds of MUC2 dimers, these proteolytic cleavages do not dissolve the network. Instead, the cleavages allow the network to expand without falling apart⁷.

In the stomach and colon, these two mucous layers are easily distinguishable. However, in the small intestine, the mucous surface is discontinuous along the length of the

small intestinal wall⁹. In the Atuma et al. 2001 *in vivo* study on rats, the firmly adherent layer of the small intestine was very thin ($\sim 20 \mu\text{m}$) or absent on individual villi

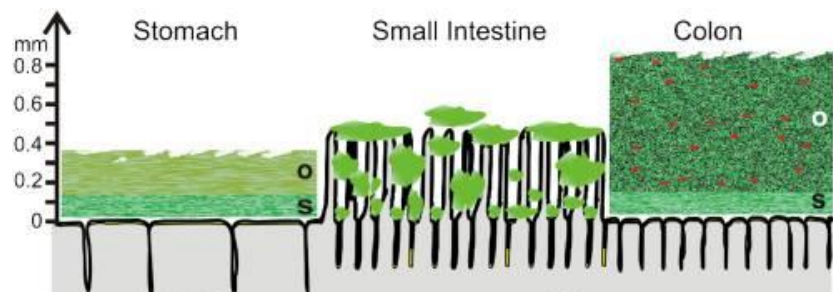


Figure 2. Mucous layers in the gut of a rat⁷. Thickness measurements adapted from Atuma et al. 2001⁹. The stomach and colon have an outer (o) loosely adherent layer and an inner stratified (s) firmly adherent layer. In contrast, the small intestine has patches of mucus that are discontinuous and ill-defined.

(Figure 2). In contrast, the firmly adherent layer was continuous and thicker in the colon ($\sim 116 \mu\text{m}$) and the corpus of the stomach ($\sim 80 \mu\text{m}$). Thus, the MUC2 network is sparser in the small intestine than in the colon.

2.3 Mucus variability. Due to the disruption of the environment when harvesting mucus samples, properties, including mechanical properties, of *in vivo* experiments may differ

from native *in vivo* mucus^{9,10}. Increased mucus secretion *in vivo* may occur in response to irritation⁹. Previous historical methods of studying mucus *in vitro* use organic fixatives and extensive dehydration which cause major shrinkage of the mucous layers¹¹⁻¹³. In all mucus experiments, mucin secretion rate, pH, and mechanical shear forces are all changed during sample collection. Hence, we do not know the actual properties of *in vivo* mucus. These factors affect the thickness, density, and other physical properties of the MUC2 network¹⁰. The difficulty of harvesting *in vivo* mucus motivates *in vitro* experiments with synthetic solutions that mimic mucus.

Since the viscoelasticity of mucus is dependent on a variety of environmental factors unique to an individual organism, viscoelastic estimates from intestinal mucus studies are widely varied. The MUC2 network is primarily responsible for the viscoelastic properties of mucus, but the viscoelasticity is also modified by water, lipid, and ion concentrations¹⁰. The thickness and viscoelasticity of the mucous layers depend on an individual's diet, which affects the gut microbiota¹⁴ and pH¹⁵.

2.4 Characterization of viscoelastic properties. As a complex (non-Newtonian) viscoelastic material, mucus exhibits both viscous (resistance to flow) and elastic (stiffness) behavior in its deformation when a shear force is applied¹⁶. An ideal elastic solid will deform to an extent when a force is applied, then the solid will immediately return to its original state when the force is removed. In contrast, an ideal viscous fluid will deform without limit when a force is applied, then the fluid will remain in the deformed state when the force is removed. Real materials are not ideal solids or ideal fluids, but rather viscoelastic materials such as mucus. In oscillatory measurements of viscoelastic mucus, a strain (γ) is applied at a

frequency (ω), and the stress (σ) is measured. For small strain, the stress is proportional to the strain (linear response) and given by

$$\sigma(t) = G' \gamma_0 \sin(\omega t) + G'' \gamma_0 \cos(\omega t) \quad (1)$$

From equation 1, $G'(\omega)$ is the storage shear modulus that quantifies the elastic component, and $G''(\omega)$ is the loss shear modulus that quantifies the viscous component.

A frequency sweep is a plot which shows $G'(\omega)$ and $G''(\omega)$ as a function of shear frequency. Viscoelastic materials are typically classified as either fluids or gels. At low frequencies, a gel has $G'(\omega)$ is greater than $G''(\omega)$, indicating that the material is more elastic than viscous. The gel will not flow in response to a small shear force. For systems characterized by a single time scale, the crossover frequency at which $G'(\omega) = G''(\omega)$ is the inverse of relaxation time τ , which is the characteristic time taken for the material to relax to its original state after a shear force is removed. For gels at high frequencies, $G'(\omega)$ is typically smaller than $G''(\omega)$, indicating that the material is more viscous than elastic. For intestinal mucus, the firmly adherent layer forms a viscoelastic gel while the loosely adherent layer forms a viscoelastic fluid¹⁷. Viscoelastic fluids have $G''(\omega)$ greater than $G'(\omega)$ at low frequencies.

A flow curve uses rotational measurements to plot viscosity as a function of shear rate. In a rotational measurement, the top plate of a rheometer will continuously rotate in the same direction rather than oscillate around an equilibrium point. A flow curve plot determines if the material is Newtonian, shear thickening, or shear-thinning. A Newtonian fluid has constant viscosity independent of shear rate. A shear thickening material has a

viscosity that increases at high shear rates. In contrast, a shear-thinning material has a viscosity that decreases at high shear rates.

2.5 Rheological measurements of mucus. Most biological fluids, such as mucus, show shear-thinning behavior¹⁶. In the firmly adherent layer, MUC2 molecules entangle and cross-link to form a viscoelastic gel with shear-thinning properties. Lai et al. 2009¹⁰ reported the range of rheology measurements of pig intestine mucus from two studies^{18,19}: in the shear rate range of 10^{-2} - 10^2 $\text{rad}\cdot\text{s}^{-1}$, viscosity = 63-5000 $\text{mPa}\cdot\text{s}$, $G' = 0.19$ -12 Pa, $G'' = 0.18$ -10 Pa. These two studies are included in a more comprehensive systematic review by Sardelli et al. 2019²⁰. Figure 3 and Table 1 (adapted from Sardelli et al. 2019) show rheological values from studies on small intestinal mucus.

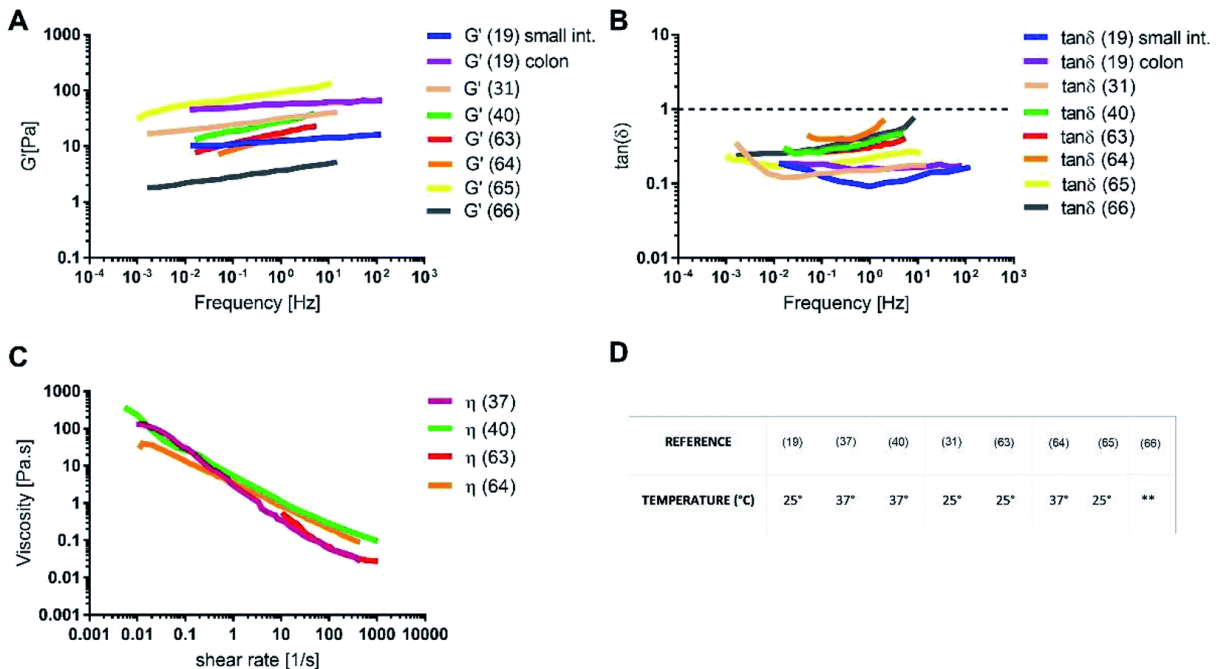


Figure 3. Rheological measurements of small intestine mucus from multiple studies, compiled by Sardelli et al. 2019. **(A)** Storage modulus (G'), **(B)** $\tan(\delta) = G''/G'$, **(C)** viscosity, and **(D)** the temperature of the rheological measurement. Reference numbers in parentheses refer to the references in Table 1.

Table 1. References used in Sardelli et al. 2019. The small intestine consists of three sections: duodenum, jejunum, and ileum.

Reference number in Sardelli et al. 2019	Reference	Mucus source
19	Sellers et al. 1991 ¹⁸	Small intestine, colon
31	Bell et al. 1985 ²¹	Duodenum
37	Macierzanka et al. 2014 ²²	Jejunum
40	Boegh et al. 2014 ²³	Jejunum
63	Meldrum et al. 2018 ²⁴	Duodenum
64	Macierzanka et al. 2011 ²⁵	Jejunum
65	Nordgard et al. 2015 ²⁶	Small intestine
66	Sellers et al. 1987 ¹⁹	Small intestine

2.6 Hydrodynamic model of Giardia attachment. For incompressible Newtonian fluids, the Navier-Stokes equation describes the motion of viscous fluids

$$\rho \frac{\partial \vec{v}}{\partial t} + \rho(\vec{v} \cdot \nabla)\vec{v} = -\nabla p + \eta \nabla^2 \vec{v} \quad (2)$$

where ρ is the density of the fluid, η is the viscosity of the fluid, \vec{v} is the flow velocity, t is time, and p is pressure.

The ratio of inertial forces to viscous forces for a moving object in a fluid is given by the Reynolds number

$$Re = \frac{F_{inertial}}{F_{viscous}} = \frac{\rho LU}{\eta} \quad (3)$$

where Re is the Reynolds number, L is the length scale of the object, and U is the velocity of the object. The Reynolds number is derived by taking the ratio of the inertial term ($\rho(\vec{v} \cdot \nabla)\vec{v}$) and the viscous term ($\eta \nabla^2 \vec{v}$) from the Navier-Stokes equation (2). *Giardia* in water and in mucus has a low $Re \ll 1$ due to the small width of the ventral groove (5 μm) and the low velocity of *Giardia* swimming (50 $\mu\text{m}\cdot\text{s}^{-1}$). Low Re systems have negligible

inertial forces and dominant viscous forces where the kinetic energy of the system dissipates to friction quickly, and thus inertial motion stops across short distances.

Therefore, for $Re \ll 1$, the Navier-Stokes equation (2) simplifies to

$$\nabla p = \eta \nabla^2 \vec{v} \quad (4)$$

Velocity at any point in time only depends on the boundary conditions at that time and not at another time. Thus, the $\rho \frac{\partial \vec{v}}{\partial t}$ term from equation (1) simplifies to 0. In low Re systems, inertial forces are negligible so the $\rho(\vec{v} \cdot \nabla)\vec{v}$ term approximates to 0.

Giardia exists in a low Re system, and thus attachment is due mostly to viscous forces, not inertial forces. Rheological measurements of mucus-analog fluids should also be in the $Re \ll 1$ regime where simple laminar flow occurs without turbulent flow.

Peristalsis in the gut provides a mechanical shear force that modifies the mucous layers. *Giardia* trophozoites must also resist peristaltic forces by residing in viscoelastic mucus and attaching to the surface of epithelial cells. Attachment is crucial for reproduction and survival.

According to the proposed hydrodynamic model of attachment which presumes a low Re regime, *Giardia* attaches via flagellar-driven fluid flow^{27,28}. Due to the pumping of the ventral flagella, fluid enters under the ventral disk at the anterior opening, and fluid is pumped out the posterior end of the ventral groove (Figure 4). Due to this

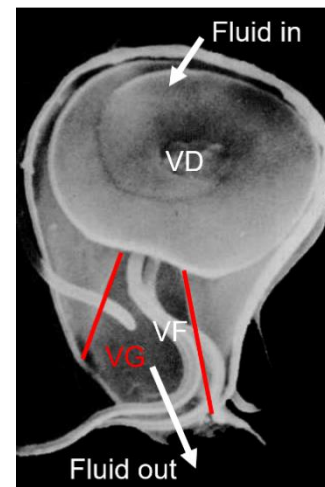


Figure 4. SEM of *Giardia* ventral surface.²⁹ Fluid flows into the cell from the anterior opening of the ventral disk (VD), and fluid is pumped out the posterior side of the ventral groove (VG) outlined in red. The ventral flagella (VF) creates this fluid-driven flow via a lower pressure area under the VD.

directed fluid flow, the pressure under the ventral disk is lower than the outside environment, creating a force sufficient for attachment.

2.7 Long Chain Polyacrylamide (LCPAM) in media. Traditional *Giardia* culture media provides the proper biochemical nutrients for *Giardia* to grow, but the media has water-like, low viscoelasticity, unlike intestinal mucus. By weight, mucus of the small intestine is comprised of 84% water and 0.7-5.8% mucins²⁰, high molecular weight glycoproteins such as MUC2. Although the concentration of mucins is low, small differences in this concentration may cause significant changes in mucus viscoelasticity. The media lacks mucins, and thus the media lacks the viscoelastic properties of mucus. To mimic the physical properties of mucus without significantly altering the biochemical pathways of *Giardia* metabolism, a high molecular weight (18 MDa) long-chain polyacrylamide (LCPAM) was added to the media. LCPAM is a water-soluble, nonionic polymer formed from acrylamide subunits ($\text{CH}_2\text{CHCONH}_2$). Uncharged LCPAM should have minimal chemical interactions with the ionic media and the anionic surface of *Giardia*³⁰. The LCPAM used in this study has a simple linear-chain structure without cross-links. Due to the high molecular weight, LCPAM enhances the viscosity and elasticity of the solvent³¹. LCPAM 18 MDa is also an appropriate analog for mucin as its molecular weight is the same order of magnitudes as MUC2 (2.7 MDa³² to 7 MDa³³).

2.8 LCPAM sonication. Sonicating the LCPAM solution via ultrasound degradation breaks the LCPAM molecules into smaller polymers. This procedure allows for decreasing the

viscosity of an LCPAM solution while keeping the concentration of LCPAM constant. A higher degree of degradation indicates that the sonicated polymer has a lower average molecular weight. In a study on the xanthan gum polymer by Saleh et al. 2017, the degree of degradation decreases with salt concentration³⁴ and polymer concentration³⁵, and it increases with sonication intensity³⁴, irradiation time^{34,36}, and molecular weight^{34,35}.

Degradation of the polymer is due to cavitation, which is harder to achieve in solutions with a high polymer concentration. When initiating liquid cavitation via sonication, the negative pressure generated by the acoustic wave in the rarefaction cycle must overcome the cavitation threshold: the natural cohesive forces holding the solution together³⁷. As the polymer concentration increases, the viscosity increases, and the magnitude of the cohesive forces increases resulting in a higher cavitation threshold. Therefore, the degree of degradation is lower in solutions with a high polymer concentration.

The presence of salts decreases the degree of degradation. As salt concentration increases, the ionic strength of the solution increases, resulting in a reduced intramolecular charge repulsion within a polymer. The contour length^{38,39} (maximum polymer length) and the persistence length³⁴ (stiffness parameter) decrease, thus decreasing rigidity and causing the polymer to collapse into a coiled state (Figure 5). The resulting coiled polymer has a lower surface area exposed

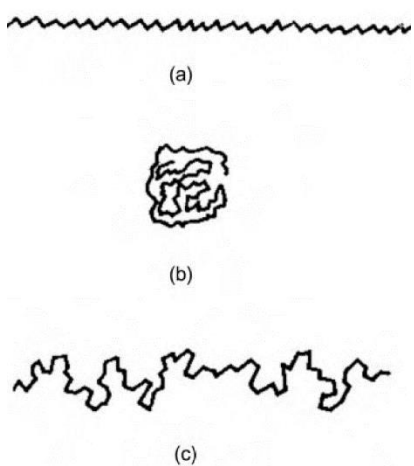


Figure 5. Configuration states for a polymer in solution³⁷. **(a)** stretched out, **(b)** coiled, **(c)** intermediate.

to extreme shear forces, leading to a lower degree of degradation in a salt solution³⁴.

3. Methods

3.1 Preparing solutions of LCPAM in media. The TYI-S-33 *Giardia* culture media was prepared with 0.024 M sodium bicarbonate substituted for the phosphate buffer solution⁴⁰. Long-chain polyacrylamide (LCPAM) 18 MDa (International Laboratory USA) was aseptically added to the media in 3 additions to create concentrations of 0.2% and 0.4% by molecular weight. Tubes were filled by balancing the max volume of liquid media with the minimum empty tube volume such that the LCPAM powder could mix properly without clumping; 40 mL of solution was prepared in a 50 mL tube. LCPAM solutions were mixed in an end-over-end rotator overnight.

3.2 Sonicating solutions. LCPAM solutions were sonicated to decrease the viscosity to the desired value. All sonication instruments that entered the tissue culture hood were sterilized with 70% ethanol (Figure 6). With 40 mL of 0.2% or 0.4% LCPAM in a 50-mL conical tube on a beaker of ice, the Sonic Dismembrator Ultrasonic Processor FB-120 (Fischer Scientific) 1/4" probe tip was submerged such that the end of the tip was in the middle of the solution volume. Solutions were sonicated for 5 seconds on, 5 seconds off at 50% amplitude (50 μ m) and 20 kHz frequency for 1-30 minutes. The

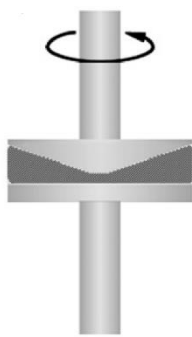


Figure 6. Sonication setup under tissue culture hood. The ultrasonic processor head is stabilized by ring stand. LCPAM solution is stabilized by a Styrofoam base and submerged in a beaker of ice.

ultrasonic processor automatically adjusted the power to maintain a constant amplitude regardless of changes in fluid's resistance to probe movement (viscosity). By keeping amplitude constant throughout the sonication process, sonication results are reproducible among solutions with varying viscosities.

Sonicated solutions were degassed to ensure an anaerobic environment for *Giardia*. A vacuum desiccator was used to eliminate oxygen bubbles from the sonicated solution. The desiccator was sterilized with 70% ethanol and placed under the tissue culture hood. The tube of the sonicated solution was uncapped, mounted on a Styrofoam base, and placed in the desiccator. The solution was degassed for 30 mins while continuously pumping with a house vacuum pump.

3.3 Measuring solution rheology. A cone and plate MCR 702 Rheometer (Anton Paar) with LPP50 and CP50 plates was used to obtain a frequency sweep and flow curve for 700 μL of each solution (Figure 7). At least 1.5 mL of each solution was aseptically collected for



rheology; this allows for at least two rheology measurements of 700 μL each. The rest of the solution was used for *Giardia* cell culture. Rheology plots were constructed with one curve per sample. A sample is defined as a solution made on a particular day. Standard deviation error bars indicate variability among multiple tests within a sample. A test is

Figure 7. Schematic of cone and plate rheometer¹⁶. A sample is loaded onto the bottom plate, and the top cone is lowered onto the sample. The top cone is rotated to perform oscillatory and steady strain rheology tests.

defined as a single set of rheology measurements from one load of 700 μL . If there were multiple

rheology measurements on the same test load of 700 μL , only one set of measurements was used to represent the test.

Rheology was measured at 37°C to mimic the temperature of the cell culture incubator. The frequency sweep was measured with 17 data points with frequency values ranging from 2 to 400 $\text{rad}\cdot\text{s}^{-1}$. Data points were equally spaced on a log scale of frequency. The flow curve was measured with 22 data points with shear rate values ranging from 0.1 to 100 s^{-1} . Data points were equally spaced on a log scale of shear rate.

Due to the rheometer's sensitivity limits, rheology data were excluded (frequency sweep: max shear rate = 30 s^{-1} , minimum torque = 100 nNm; flow curve: minimum torque = 650 nNm). For the frequency sweep, if G' was greater than G'' , the data was excluded since the rheometer was measuring surface tension due to improper sample loading technique. The calculated characteristic shear rate of *Giardia* is 10-270 s^{-1} . Therefore, a characteristic viscosity at a 10 s^{-1} shear rate was determined from the flow curve of each solution.

3.4 Culturing *Giardia* for growth curves. *Giardia* trophozoites were grown at 37°C in autoclaved 9-mL glass tubes of control media (CM), 0.2% LCPAM, or 0.4% LCPAM.

3.4.1 Cell seeding. To increase the population of *Giardia* cells, cells from one tube were seeded into multiple new tubes. First, the confluent tubes were observed under a 10x light microscope to ensure that cells were at 80-100% confluency. Tubes were chilled on ice for 15 minutes. Tubes were shaken to detach cells and cells were observed under the microscope to ensure detachment. Under a tissue culture hood, all cell solutions were

combined into a sterile 15-mL or 50-mL conical tube. The conical tube was centrifuged for 10 minutes at 2500 rpm. Under a hood, the tube was placed on ice and the supernatant was removed using a serological pipet. With a serological pipet, $3n$ mL of fresh media was added and mixed with the cell pellet where n is the number of confluent tubes used in the seeding process. $10 \mu\text{L}$ of this concentrated cell solution was transferred to a PCR tube and counted on a 0.1 mm^3 hemocytometer. The cell density of the concentration solution, d_i , should satisfy

$$d_i \geq \frac{d_f \cdot 9 \text{ mL}}{0.5 \text{ mL}} \quad (5)$$

where d_f is the final seeding cell density in each newly seeded 9 mL tube. If condition (5) is not satisfied, then cells cannot be seeded for a quantitative growth curve analysis. If condition (5) is satisfied, dilute the concentrated cell solution so that the two sides of the condition equate. To seed cells, add 0.5 mL of the concentrated cell solution into each new 9-mL tube and fill the tube with fresh media.

3.4.2 Media refreshing. Due to the build-up of cell debris and a decrease in *Giardia* nutrient supply over time, media should be refreshed (replaced with fresh media) every 3-4 days. Media refers to the solution in the tube, so media could represent CM, 0.2%, or 0.4% LCPAM. Since most living *Giardia* cells are attached when taken out of the incubator, old media and debris can be removed without removing living cells. Old media was slowly removed via a serological pipet, and fresh media was used to replenish the tubes.

3.4.3 Qualitative growth curves. In preparation for a quantitative growth curve, *Giardia* growth was initially observed qualitatively over time. Following the cell seeding procedure, tubes were seeded with a known starting cell density. Every 6, 12, or 24 hours, cell growth was observed by taking images of the ceiling and floor at 3 points along the length of the tube (total of 6 images per tube). Estimates of % confluency were recorded for each timepoint. After imaging, tubes were placed back into the incubator with the same configuration for the ceiling and floor. Qualitative growth curves were constructed based on the % confluency estimates. This preliminary data informed an estimate for the max timepoint of the quantitative growth curve experiments.

3.4.4 Counting Giardia cells. The number of cells in a tube was counted to build the quantitative growth curves. The 9-mL glass tubes were placed on ice for 20 minutes, then shaken to detach cells. Each cell solution was transferred to a separate 50-mL conical tube. To ensure sufficient transfer of cells, the interior wall of all 9-mL glass tubes was rinsed with 8 mL of cold 1x PBS and transferred to the 50-mL tube. The second and third rinse were with 5 mL of cold PBS. After rinsing, all 50-mL tubes were centrifuged at 2500 rpm for 10 minutes. A 10-mL serological pipet was used to slowly remove the supernatant until ~3.8 mL of solution is left. The pellet was resuspended by mixing in 1 mL of cold PBS. 10 μ L of the cell suspension was added to a microcentrifuge tube. The volume of the remaining cell solution (y in equation 6) was measured. In the microcentrifuge tube, 10 μ L of filtered trypan blue was added and the solution was mixed using a 10 μ L pipet. Cells were counted by loading 10 μ L of the mixed solution onto a 0.1 mm³ hemocytometer.

For each 0.1 μL hemocytometer quadrant, the number of living and dead cells were counted, and the quadrant was imaged for future reference (Figure 8). The cell density ρ [cells/mL] was calculated using

$$\rho = \frac{x \text{ cells}}{10^{-4} \text{ mL}} \cdot 2 \cdot \frac{y \text{ mL}}{9 \text{ mL}} \quad (6)$$

where x is the average number of cells per hemocytometer quadrant, y is the volume of the remaining cell solution, and the factor of 2 is the dilution factor to account for the trypan blue.

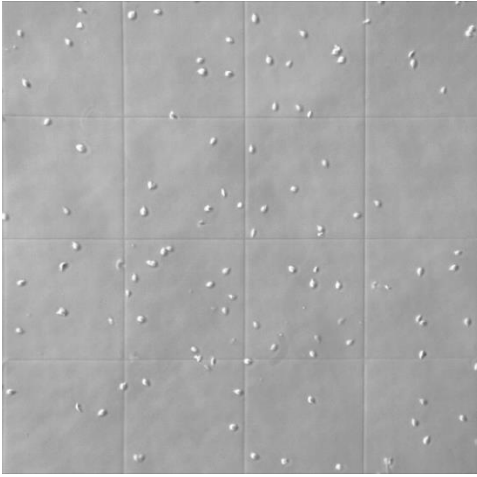


Figure 8. Image of 16-grid hemocytometer quadrant observed under a 10x light microscope. The total number of living cells was counted per quadrant. Living *Giardia* are bright, tear-dropped shaped cells while dead *Giardia* are perfectly round circles and smaller in size.

3.4.5 Quantitative growth curves. Two types of quantitative growth curve sets were constructed: (1) CM cells seeded into CM, 0.2%, and 0.4% LCPAM, and (2) 0.4% LCPAM-conditioned cells seeded into CM, 0.2%, and 0.4% LCPAM. 0.4% LCPAM-conditioned cells are cells that were maintained in a 0.4% LCPAM solution for at least 6 days.

For a quantitative growth curve assay, all tubes were seeded at the same time and at the same seeding density. Thus, before starting this experiment, the total number of tubes (n) for each solution type needs to be calculated using

$$n = a \cdot \left(1.25 \cdot \frac{t}{T} + \frac{t}{96} \right) \quad (7)$$

where t is the max timepoint from the qualitative growth curve, T is the timepoint period, and a is the number of tubes counted per timepoint. In equation (7), the factor of 1.25

accounts for extra tubes in case of contamination, and the $\frac{t}{96}$ term accounts for the additional tubes used for media refreshing every 96 hours. Table 2 shows conditions and variable values for equation (7).

After seeding the appropriate number of tubes, tubes were placed in a 37°C incubator for cell growth. At each timepoint, cells were counted quantitatively. To construct growth curves of the cell density over time, the average cell density was plotted with error bars representing standard error among hemocytometer quadrants (CM growth curves) or the standard deviation among tubes (0.4% LCPAM-conditioned growth curves).

Table 2. Conditions for CM and 0.4% LCPAM-conditioned quantitative growth curve sets. Variables in parentheses are values for equation (6). The timepoint period represents how often tubes were counted. For the CM growth curve set, tubes were counted every 12 or 24 hours, depending on the solution type.

	CM growth curve set	0.4% LCPAM-conditioned growth curve set
Seeding density [cells/mL]	9.0 x 10 ⁴	6.8 x 10 ⁴
Number of tubes counted per timepoint (a)	1	2
Cell density error bars	SE among hemocytometer quadrants	SD among tube totals
Maximum timepoint [hours] (t)	168	72
Timepoint period [hours] (T)	12 or 24	24
Media refresh timepoint	96 hours for 0.2% and 0.4% LCPAM	N/A

4. Results

4.1 Rheology of LCPAM solutions. Previous studies have investigated the rheology of LCPAM in a water solvent, so as a first step we investigated the effect of using CM as the solvent. Figure 9a shows the viscosity vs. shear rate for 0.4% LCPAM in water (green), and

the same concentration in CM (blue). At all shear rates, the viscosity is substantially lower, and the shear-thinning behavior is less dramatic. As with pure water solvents, the viscosity of LCPAM in CM increases strongly with concentration (compare 0.2%, purple, with 0.4%, blue).

To compare the elasticity of the LCPAM solutions, a frequency sweep was created from representative data of one sample of 0.4% LCPAM in water, 0.4% LCPAM in media, and 0.2% LCPAM in media (Figure 9b). All 3 solution types exhibit the behavior of a viscoelastic fluid: $G'' > G'$ at low frequencies and $G' > G''$ at high frequencies. The relaxation time τ of 0.4% LCPAM in water (59 s) is approximately 3 orders of magnitude greater than that of 0.4% LCPAM in media (0.073 s) and 0.2% LCPAM in media (0.057 s). At all frequencies, 0.4% LCPAM is more viscous (compare blue with purple triangles) and more elastic than 0.2% LCPAM (compare blue with purple circles, Figure 9b).

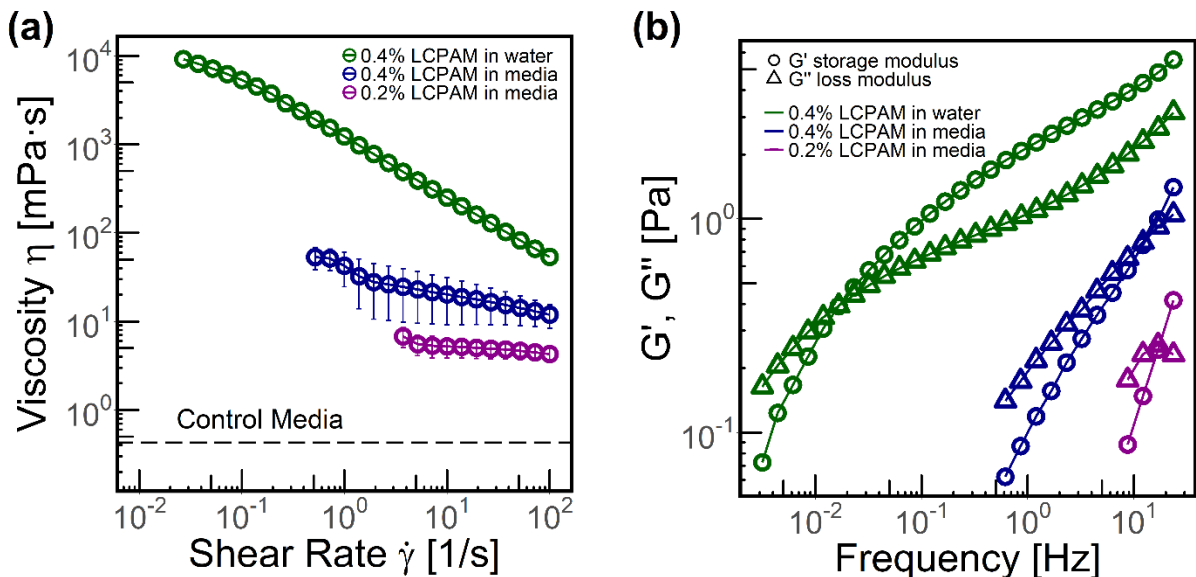


Figure 9. Flow curve (a) and frequency sweep (b) of 0.4% LCPAM in water (green, $n = 1$), 0.4% LCPAM in media (blue, $n = 7$), and 0.2% LCPAM in media (purple, $n = 3$). (a) Error bars show the standard deviation of samples. The dashed line on the flow curve indicates the viscosity of the media solvent which has the same viscosity as water ($\eta = 0.69$ mPa·s). (b) Circles are the storage modulus (G'), triangles are the loss modulus (G''). Representative data from one sample of each solution ($n = 1$) is shown.

Unless specified, 0.4% LCPAM and 0.2% LCPAM refers to LCPAM in a media solvent.

In measuring multiple samples of 0.4% LCPAM, there was high variability among sample rheology. Thus, we investigated two potential sources of variability: variability due to tests of the same sample or variability due to samples. The variability in 0.4% LCPAM is higher among samples than among tests for the same sample (Figure 10). This suggests that the rheometer produces reproducible results whereas sample preparation may not be as consistent. While the inconsistency in rheology measurements is concerning, 0.2% LCPAM does have a different viscosity than 0.4% LCPAM since the error bars of their flow curves do not overlap (Figure 9a).

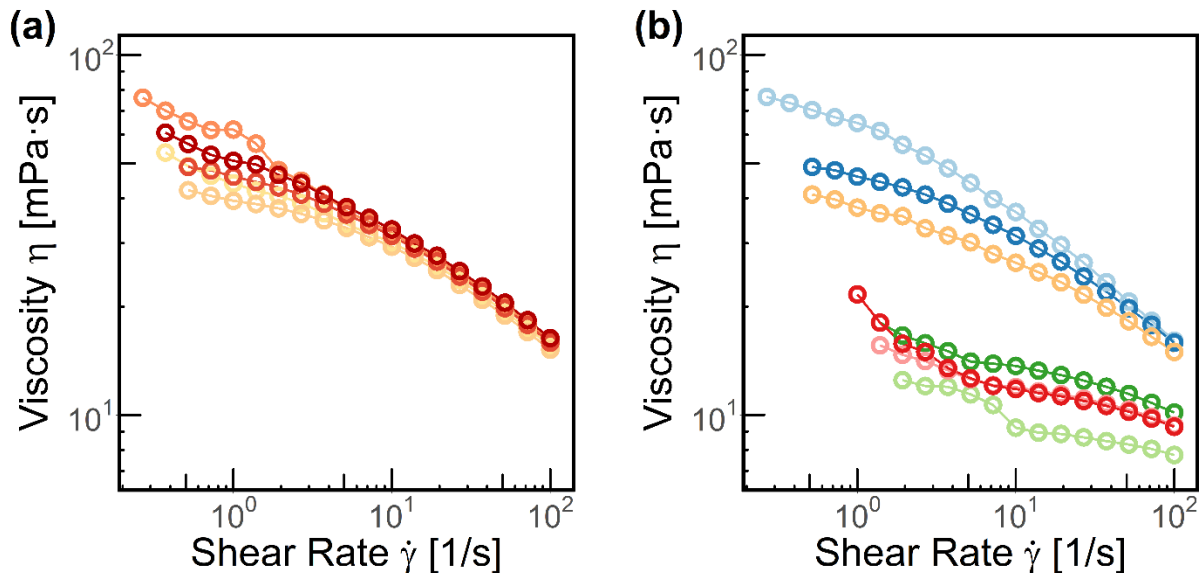


Figure 10. Flow curve of (a) five 0.4% LCPAM tests for the same sample and (b) seven 0.4% LCPAM samples. Variability in LCPAM rheology is not due to test variation (a), but rather variability is due to variation among samples (b).

4.2 LCPAM sonication rheology. To reduce the viscosity of 0.4% LCPAM without changing the concentration, we sonicated 0.4% LCPAM for 1 minute to reach a characteristic viscosity (3.44 mPa·s) similar to that of 0.2% LCPAM (5.21 mPa·s; Figure 11). Sonication times greater

than 10 minutes did not greatly affect viscosity. As sonication time increases, sonicated 0.4% LCPAM reaches a minimum viscosity of 1.18 mPa·s.

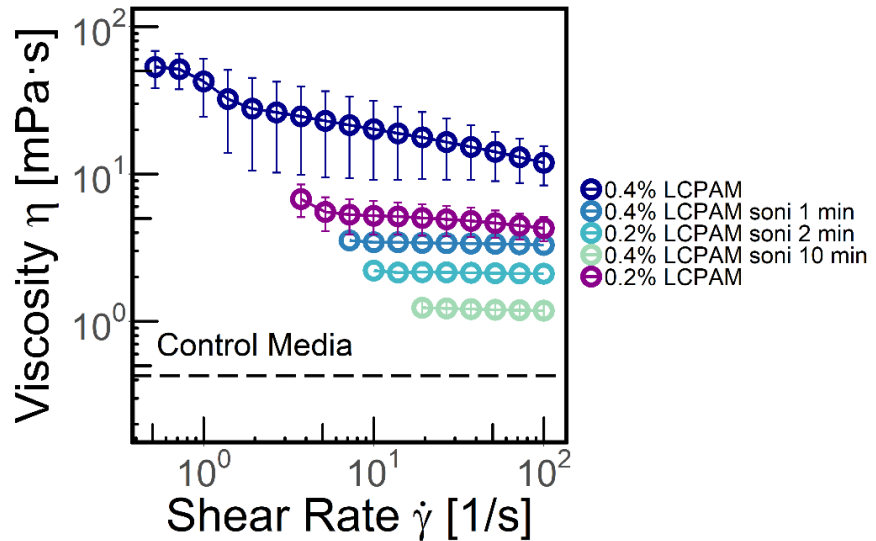


Figure 11. Flow curve of 0.4% LCPAM (dark blue, n = 7) and 0.4% LCPAM sonicated for 1 min (blue, n = 1), 2 min (light blue, n = 1), and 10 min (light green, n = 1). 0.2% LCPAM shown in purple (n = 3), and dashed line indicates media solvent viscosity ($\eta = 0.69$ mPa·s). Error bars are standard deviation of samples. 0.4% LCPAM sonicated for 1 min has approximately the same viscosities as 0.2% LCPAM.

To ensure that

sonication was affecting LCPAM viscosity and not the CM solvent viscosity,

CM without LCPAM was sonicated. Sonicating CM for 10 minutes resulted in no change in solvent viscosity.

4.3 Giardia growth curves.

4.3.1 Control cells. To test our hypothesis that viscoelastic environments affect *Giardia* growth, we measured growth curves of *Giardia* in solutions with measured rheology. First, we started with control cells grown in control media (CM), 0.2% LCPAM, and 0.4% LCPAM. Populations in all solutions reach approximately the same confluency ($\sim 1.1 \times 10^6$ cells/mL), but the time until confluency depends on the solution (CM = 72 h, 0.2% LCPAM = 120 h, 0.4% LCPAM = 168 h; Figure 12a). Cells in 0.2% LCPAM have initial growth behavior similar to CM, but after 36 hours, the growth in 0.2% LCPAM is not sustained.

The growth phase is defined as the time period where cell density sharply increases, and the growth rate is at its maximum. The lag time is defined as the time until the growth phase begins. The lag time for CM, 0.2%, and 0.4% LCPAM is 24 h, 96 h, and 144 h respectively (Figure 12a). When plotted on a lag time vs. log viscosity scale, lag time increases logarithmically as average viscosity increases (Figure 12c).

4.3.2 0.4% LCPAM-conditioned cells. After CM cells were grown in the 3 solutions, the confluent 0.4% LCPAM cells were similarly seeded into the 3 solutions. 0.4% LCPAM-conditioned cells grown in CM, 0.2%, and 0.4% LCPAM all have a lag time of 24 hours (Figure 12b). During the growth phase, 0.4% LCPAM has a faster growth rate than CM and 0.2% LCPAM which have similar growth rates.

4.3.3 Control cells vs. 0.4% LCPAM-conditioned cells. For all 3 solutions, 0.4% LCPAM-conditioned cells do not reach the confluency cell density of control cells. The lag time for control cells increases with solution viscosity whereas, for 0.4% LCPAM-conditioned cells, it is independent of the solution. The growth rate, or the slope of the growth curve during the growth phase, for control cells is independent of the solution whereas for 0.4% LCPAM-conditioned cells, it is dependent on the solution.

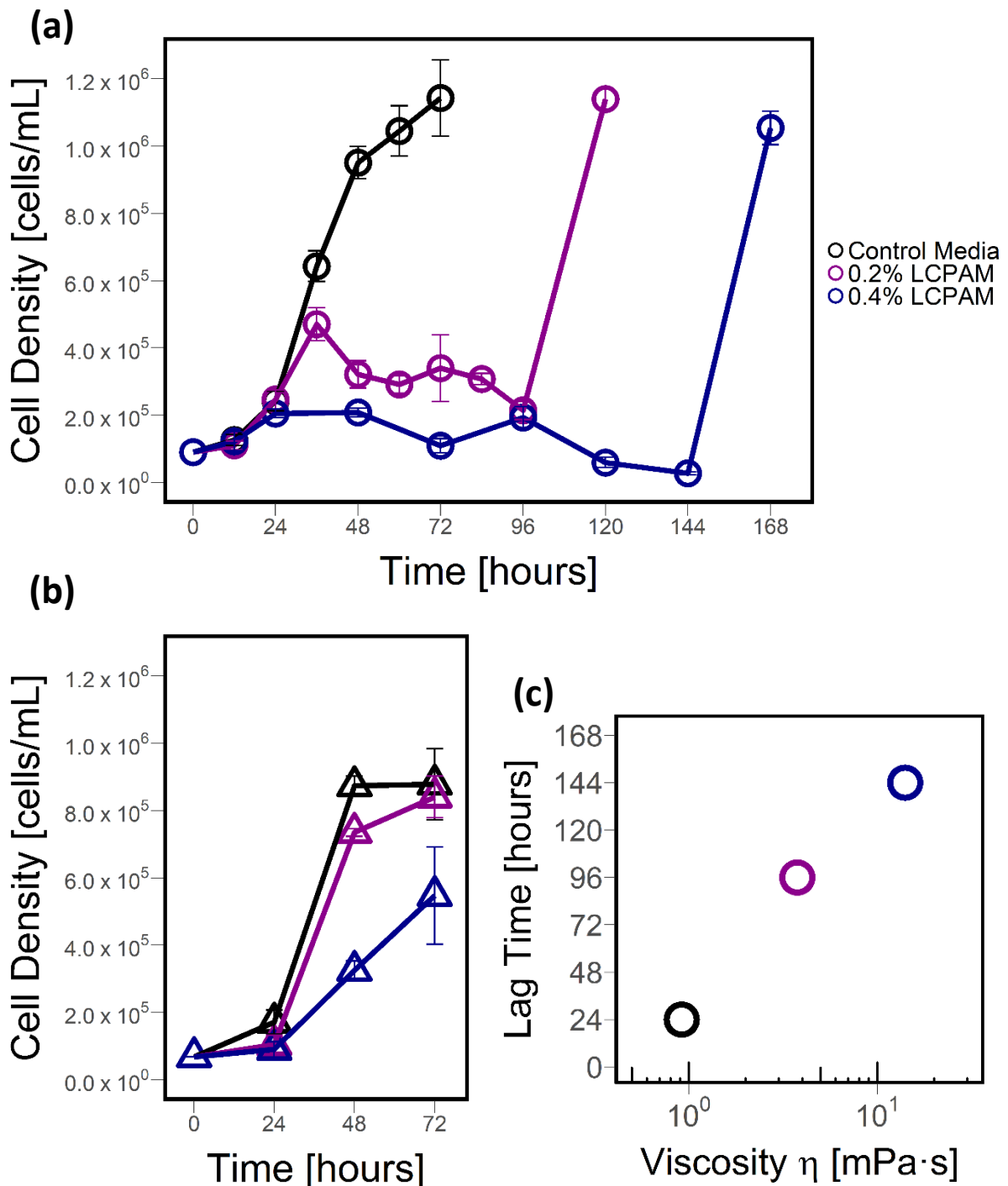


Figure 12. Growth curves of control cells **(a)** and 0.4% LCPAM-conditioned cells **(b)** grown in control media, 0.2% LCPAM, and 0.4% LCPAM. **(a)** Each point represents one tube, and error bars represent the standard error of the hemocytometer quadrants. All tubes had a starting cell density of 9.0×10^4 cells/mL. 0.2% and 0.4% LCPAM tubes were refreshed with new media at 96 hours. **(b)** Each point represents the average of two tubes, and error bars represent the standard deviation of the tubes. All tubes had a starting cell density of 6.8×10^4 cells/mL. **(c)** Lag time (extracted from panel a) vs. average viscosity for control cells grown in the 3 solutions. Average viscosity is displayed on a log scale.

5. Discussion

5.1 LCPAM in water vs. media. For the discussion that follows, viscosities at a 10 s^{-1} shear rate are compared. The characteristic viscosity of 0.4% LCPAM in a water solvent (250 mPa·s) is about 10 times greater than 0.4% LCPAM in a media solvent (20 mPa·s; Figure 9a). To explain this difference, we assess the chemical differences of water vs. media. For purposes of rheology, the primary difference is the presence of 0.4% salts in the media.

Contrary to our results, Chen et al. 2012 reported that the viscosity of 2.6 MDan LCPAM does not change in the presence of increasing salt concentrations up to 2%⁴¹. This suggests that not only the presence of salts but the interactions of salts and other macromolecules in the media contribute to the overall lower viscosity of LCPAM in media compared to water. Hypothetically, the small biomolecules in the media (i.e. peptones and yeast extracts) could reduce the LCPAM intermolecular reactions and increase the affinity for intramolecular H-bonding of the LCPAM amides. This would cause the linear LCPAM molecule to collapse into a coiled state (Figure 5). LCPAM in a coiled state decreases the entanglement between LCPAM molecules, leading to a decrease in viscosity. While this biochemical reasoning may be true, overall, the mechanism to explain the reduced viscosity and increased elasticity of 0.4% LCPAM in media vs. in water is unknown.

Our 0.4% LCPAM in media does not mimic all the properties of mucus, but we can investigate analogies between our viscoelastic salty solution and mucus. Salts account for up to 1% of mucus mass^{10,42,43}. An increase in ion concentration correlates with a decrease in mucus viscosity¹⁰, which is a similar trend observed in our comparison of 0.4% LCPAM in salty media vs. in non-salt water (Figure 9a). In mucus, an increase in ion concentration

correlates with more elastic behavior⁴⁴. This relationship is not apparent in our comparison of 0.4% LCPAM in salty media vs. in water. Instead, at all shear rates 0.4% LCPAM in media has a lower storage modulus (G') than 0.4% LCPAM in water, indicating that 0.4% LCPAM in media is less elastic.

5.2 0.2% vs. 0.4% LCPAM in media. The viscosity of LCPAM is dependent on concentration.

To explain the intermolecular interactions between LCPAM molecules, the overlap concentration was calculated by finding the critical concentration where the average spacing between molecules equals R_g .

$$\frac{V_p}{V_s} = \frac{N_p \cdot \left(\frac{4}{3}\pi R_g^3\right)}{V_s} = 1 \quad (8)$$

$$c_{critical} = \frac{N_p \cdot \bar{M}_w}{V_s} \quad (9)$$

$$c_{critical} = \frac{3\pi}{4} \cdot \frac{\bar{M}_w}{R_g^3} \quad (10)$$

In equations (7-9), V_p is the volume of the solute particles, V_s is the volume of the solution, N_p is the number of solute particles, R_g is the radius of gyration, \bar{M}_w is the molecular weight of the solute, and $c_{critical}$ is the critical overlap concentration. In equation (10), the overlap concentration can be simplified to a function of \bar{M}_w and R_g . For our 18 MDan LCPAM in media, the R_g is approximately 350 nm^{45,46} and thus the overlap concentration is 0.017% LCPAM.

Since the 0.4% LCPAM solution is notably greater than the critical overlap concentration, the LCPAM molecules will entangle with each other via intermolecular forces. For shear-thinning fluids such as 0.4% LCPAM, the applied shear force is both stretching the coiled LCPAM (weakening intermolecular forces) and detangling the coils

(weakening intermolecular forces). Detangling has a greater effect on viscosity, so we see the shear-thinning effect in the viscosity vs. shear rate plot for 0.4% LCPAM (Figure 9a, blue). As a greater shear force is applied, the coils are detangled more and thus the viscosity decreases.

The 0.2% LCPAM solution has a concentration greater than but close to the overlap concentration of 0.017%. Thus, 0.2% has less shear-thinning behavior as observed in Figure 9a, purple. The viscosity vs. shear rate curve of 0.2% LCPAM appears Newtonian-like because the starting viscosity is low and close to the Newtonian solvent viscosity. At low shear rates, the LCPAM additive does not change the viscosity very much. Thus, the effect of reducing the LCPAM's contribution at high shear rates is negligible.

5.3 0.4% LCPAM vs intestinal mucus. The rheology of our 0.4% LCPAM analog is lower than that of intestinal mucus. In the shear rate range of 10^{-2} - 10^2 $\text{rad}\cdot\text{s}^{-1}$, the viscosity of mucus from a pig small intestine ranged from 63 to 5000 $\text{mPa}\cdot\text{s}$ ^{10,18,19}; the range for our 0.4% LCPAM viscosity (11-53 $\text{mPa}\cdot\text{s}$, Figure 9a) is lower than the range of the reference small intestine mucus. In comparison to viscosity values of intestinal mucus from the recent systematic review Sardelli et al. 2019²⁰, our 0.4% LCPAM in water has a viscosity vs. shear rate curve that is the most similar to the mucus references (compare green dashed with solid curves, Figure 13). Although our 0.4% LCPAM in media has a lower viscosity than small intestine mucus samples at all shear rates (compare blue dashed with solid curves, Figure

13), 0.4% LCPAM in media still serves as an appropriate mucus analog in that it exhibits the shear-thinning behavior of mucus with a significantly higher viscosity than water (Figure 9a).

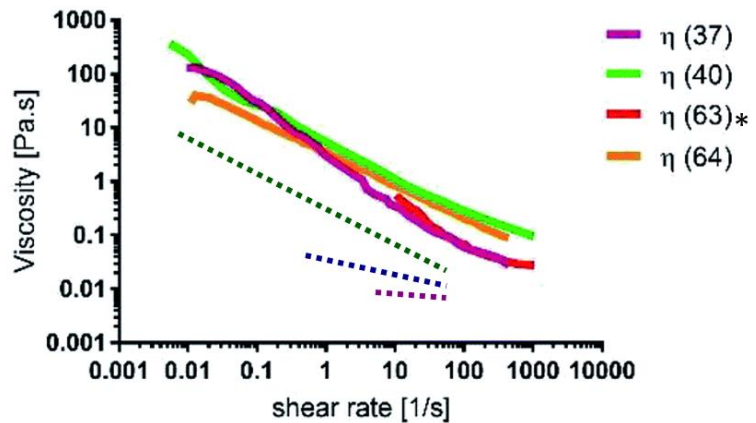


Figure 13. Flow curves of this study's 0.4% LCPAM in water (green dashed), 0.4% LCPAM in media (blue dashed), and 0.2% LCPAM in media (purple dashed) overlaid on intestinal mucus samples from the systematic review Sardelli et al. 2019²⁰. The citation reference number from the Sardelli study is in parentheses. Reference 63 refers to the Meldrum et al. 2018²⁴ study of pig mucus in the duodenum, the primary region of *Giardia* infection. References 27, 40, and 64 studies mucus in the jejunum, another region of the small intestine.

5.4 LCPAM rheology

variability. The wide rheology

variability among LCPAM samples may be due to a variety of factors. We qualitatively observed that 0.4% LCPAM precipitates out of solution in some samples. The supernatant is less viscous than the bottom of the tube due to the collection of LCPAM debris. This suggests that a 0.4% concentration is too high for LCPAM to be fully mixed. The concentration of LCPAM is not uniformly distributed along the length of the tube. For example, for a prepared 0.4% LCPAM solution, the bottom of the tube may be 0.5% LCPAM and the top of the tube may be 0.3% LCPAM. Thus the rheology of each sample will vary depending on the location of sample collection within the tube.

LCPAM variability could also be attributed to factors outside the limits of our experimental design. For example, while in theory each batch of media is prepared in an identical manner, the bovine sera and bile components are derived from different cows, and the ultrapure water quality varies by week. The variability is inevitable when studying

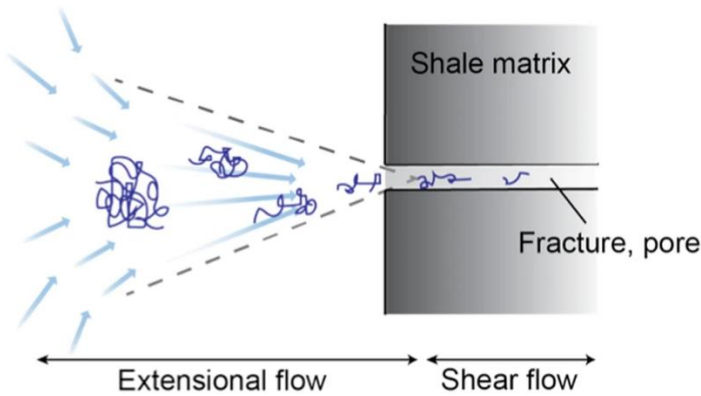


Figure 14. Mechanical degradation of LCPAM through a narrow pore⁴⁸. Schematic is comparable to pipetting an LCPAM solution sample into the rheometer. As LCPAM coils funnel through the narrow pore, the intramolecular interactions are weakened, and LCPAM transitions to a linear state.

living, biological organisms that live in ultrapure water, such as *Giardia* and other bacterial populations⁴⁷. Moreover, the LCPAM solution measured in the rheometer could have been put under additional mechanical stress due to pipetting (Figure 14). Thus, the viscosity and elasticity of the measured sample

may be lower than the actual LCPAM solution in which the *Giardia* are growing.

5.5 LCPAM sonication. Sonicating 0.4% LCPAM was successful in decreasing the viscosity. Sonicating 0.4% LCPAM for 1 minute yielded approximately the same viscosity as 0.2% LCPAM (Figure 11). In this study, massive *Giardia* cell death within 12 hours was observed when seeding cells in a 10-minute-sonicated 0.4% LCPAM without degassing. This suggests that even when bubbles are not visible in the solution, the sonication procedure introduces dissolved gas or gas bubbles that are lethal to anaerobic *Giardia*. Degassing after sonication is a crucial step in preparing a viable solution for *Giardia*.

Qualitatively, *Giardia* growth in sonicated 0.4% LCPAM yields variable results: *Giardia* sometimes exhibits growth behavior similar to its growth behavior in an un-sonicated solution with the same viscosity, and *Giardia* sometimes enters a long death phase in which the population does not recover. This inconsistency in *Giardia* growth

suggests that sonicating LCPAM in media is not a chemically inert process. Breaking down polymer chains may generate free radicals, which introduce a new chemical effect that could potentially be lethal for *Giardia*. If this chemical change does occur during sonication, then sonication is counter-effective. Sonication was executed to test the hypothesis that the addition of LCPAM does not have a chemical effect on the media. However, if sonication is introducing a new chemical effect, then we cannot isolate the physical effect of LCPAM from its chemical effect.

5.6 Adaptation vs. acclimation. To explain the difference in growth curves in Figure 12a and Fb, we evaluate two hypotheses: adaptation vs. acclimation. Adaptation is equivalent to the theory of natural selection or biological evolution. If this hypothesis is true, *Giardia* will select for phenotypes that are advantageous in the new environment, and cells with this phenotype will replicate while cells without the phenotype will die. In contrast, acclimation is equivalent to epigenetics. If this hypothesis is true, individual *Giardia* cells will alter their gene expression to adapt to the new environment. Acclimation is adjustment within the lifetime of an individual cell, and adaptation is the adjustment of the population over multiple generations. For biological organisms, the adjustment to a new environment is typically a combination of both acclimation and adaptation. When *Giardia* are placed in a high-stress environment (0.4% LCPAM), *Giardia* eventually adjust to their new viscoelastic environment via adaptation or acclimation.

The rapid growth during all growth phases in Figure 12a and Fb suggest that acclimation is dominant over adaptation. Adaptation requires multiple lifecycles to achieve,

and *Giardia* undergoes replication every 6 to 8 hours in CM. Thus, if adaptation were the dominant mechanism, we would expect to see a gradual increase in cell density over time. Instead, we observe rapid growth within 24 hours for *Giardia* in 0.2% and 0.4% LCPAM. This rapid growth is better explained by a sudden change in gene expression by all cells in the solution. As soon as *Giardia* adopts the proper gene expression, *Giardia* can quickly replicate and thrive in their viscoelastic environment. Moreover, adaptation is not likely since there are extremely low levels of genetic variation in *Giardia* populations⁴⁹. This suggests that random mutations are rare, and thus *Giardia* does not have much genetic diversity to selectively favor a particular phenotype within a population.

To further distinguish between adaptation vs. acclimation, two types of experiments can be done: (1) genetic sequencing and (2) reversion growth curves. For the first experiment, we would compare the genome and transcriptome of CM cells grown in 0.4% LCPAM at seeding vs. at confluency. If the genome is more different than the transcriptome, then adaptation is dominant; acclimation is dominant if vice versa. For the second experiment, CM cells will be grown to confluency in 0.4% LCPAM, then these 0.4% LCPAM-conditioned cells will be grown to confluency in CM, then these 0.4%-to-CM cells will be grown in 0.4% LCPAM. If the resulting cells exhibit a growth curve similar to CM cells in CM, then *Giardia* retains full genetic memory after initial adaptation to 0.4% LCPAM. On the other hand, if the resulting cells exhibit a growth curve similar to CM cells in 0.4% LCPAM, the *Giardia* has a time-limited genetic memory in which cells acclimate to their current environment independent of their previous environments. The second proposed

experiment is easier to execute than the first, and thus Figure 12b represents the 0.4% LCPAM-conditioned cells grown in CM.

Qualitatively, we observed that the 0.4%-to-CM cells grown in 0.4% LCPAM had a lag phase of 144 hours and a growth curve similar to CM cells grown in 0.4% LCPAM (Figure 12a,b, blue). Thus, these results support the hypothesis that acclimation is dominant over adaptation.

5.7 Future studies. With an experimental question as complex as the one this study aims to investigate, a wide array of future studies can be suggested to understand the growth of *Giardia* in viscoelastic fluids. In this section, a few potential experiments are proposed in the order of increasing significance.

To address the problem of high rheology variability among LCPAM samples, another polymer, with similar physical properties of LCPAM, should be tested. The heterogeneous concentration of LCPAM within a tube due to insufficient mixing leads to weak conclusions on the effect of viscoelasticity on *Giardia* growth. Thus, we want to find a different polymer that fits the following criteria for a mucus analog: (1) increases the viscoelasticity or viscosity of the solution, (2) has minimal chemical modifications to the media solvent or *Giardia*, and (3) creates a homogenous concentration when mixed with media. Xanthan gum is a polysaccharide that may satisfy these criteria. The methodology of this study should be repeated with xanthan gum instead of LCPAM.

Given that the reversion growth curves suggest acclimation as dominant over adaptation, RNA sequencing should be done on cells cultured in CM and 0.4% LCPAM-

conditioned cells. This genetic analysis may provide further evidence to support the acclimation theory.

To put this study in the context of *Giardia* infection, an experiment can be done to observe the onset and severity of giardiasis in mice infected with CM cells vs. 0.4% LCPAM-conditioned cells. Based on this study's results, we hypothesize that giardiasis onset will occur earlier in infections of 0.4% LCPAM-conditioned cells since these cells are adjusted to the viscoelasticity of intestinal mucus.

The hydrodynamic model of *Giardia* attachment can be further supplemented with experimental observations of flagellar pumping and fluid flow in viscoelastic solutions. The current hydrodynamic model proposes experimental and theoretical mechanisms for *Giardia* attachment in water, but modeling the waveform of the flagella in a viscoelastic solution can improve the relevance of the model for *Giardia*'s mucous, infectious environment.

6. Conclusion

Previous studies investigated *Giardia* in a water-like environment, but *Giardia*'s infectious environment is viscoelastic intestinal mucus. Thus, LCPAM was added to the water-like media in concentrations of 0.2% and 0.4% to yield a viscoelastic solution compatible with *Giardia* growth. A sonication protocol was created to effectively reduce the viscosity of 0.4% LCPAM to that of 0.2% LCPAM and CM. With future modifications, sonicated LCPAM solutions can be used to eliminate the physical effect (reduce viscoelasticity) and observe the chemical effect on *Giardia* growth.

Giardia growth was observed over time in solutions of CM, 0.2%, and 0.4% LCPAM. The lag time before the growth phase was greater in higher viscosity solutions, but the growth phase of all 3 solutions are approximately identical. Along with quantitative and qualitative reversion growth curves, these growth curve trends suggest that *Giardia*'s adjustment to viscoelasticity is primarily acclimation rather than adaptation.

Acknowledgements

Most importantly, I would like to thank the people who made this research project possible. To the principal investigators Professor Jeff Urbach and Professor Heidi Elmendorf, thank you for welcoming me to the *Giardia* team. Thank you for supporting and encouraging my intellectual curiosity. Your constant guidance and feedback were invaluable to the development of this thesis and its ideas. To Claire Li, thank you for all your diligent work in maintaining the *Giardia* cultures, especially when our 12-hour timepoints required late nights and early mornings in the lab. Your commitment to research sparks my excitement for the future of science. To Dr. David Gagnon, thank you for sharing your immense knowledge of fluid dynamics and rheology. The theoretical modeling and depth of physical explanations would not be possible without your mentorship. To Professor Sarah Marzen, thank you for advising this thesis from a biophysics view. Your support is greatly appreciated and valuable in finalizing this thesis.

This project was supported by NSF grant number DMR-1659532 for the Georgetown Material Physics Research Experience for Undergraduates (REU) 2019.

Literature Cited

- 1 Rendtorff, R. C. The experimental transmission of human intestinal protozoan parasites. II. Giardia lamblia cysts given in capsules. *Am J Hyg* **59**, 209-220, doi:10.1093/oxfordjournals.aje.a119634 (1954).
- 2 Huang, D. B. & White, A. C. An updated review on Cryptosporidium and Giardia. *Gastroenterol Clin North Am* **35**, 291-314, viii, doi:10.1016/j.gtc.2006.03.006 (2006).
- 3 Kappus, K. D., Lundgren, R. G., Jr., Juranek, D. D., Roberts, J. M. & Spencer, H. C. Intestinal parasitism in the United States: update on a continuing problem. *Am J Trop Med Hyg* **50**, 705-713, doi:10.4269/ajtmh.1994.50.705 (1994).
- 4 Adam, R. D. Biology of Giardia lamblia. *Clin Microbiol Rev* **14**, 447-475, doi:10.1128/CMR.14.3.447-475.2001 (2001).
- 5 Chin, A. C. *et al.* Strain-dependent induction of enterocyte apoptosis by Giardia lamblia disrupts epithelial barrier function in a caspase-3-dependent manner. *Infect Immun* **70**, 3673-3680, doi:10.1128/iai.70.7.3673-3680.2002 (2002).
- 6 Prevention, C. f. D. C. a. *Giardia Pathogen and Environment*, <<https://www.cdc.gov/parasites/giardia/pathogen.html>> (2017).
- 7 Johansson, M. E. V., Larsson, J. M. H. & Hansson, G. C. The two mucus layers of colon are organized by the MUC2 mucin, whereas the outer layer is a legislator of host–microbial interactions. *Proceedings of the National Academy of Sciences* **108**, 4659-4665, doi:10.1073/pnas.1006451107 (2011).

- 8 Allain, T., Amat, C. B., Motta, J. P., Manko, A. & Buret, A. G. Interactions of *Giardia* sp. with the intestinal barrier: Epithelium, mucus, and microbiota. *Tissue Barriers* **5**, e1274354, doi:10.1080/21688370.2016.1274354 (2017).
- 9 Atuma, C., Strugala, V., Allen, A. & Holm, L. The adherent gastrointestinal mucus gel layer: thickness and physical state in vivo. *Am J Physiol Gastrointest Liver Physiol* **280**, G922-929, doi:10.1152/ajpgi.2001.280.5.G922 (2001).
- 10 Lai, S. K., Wang, Y. Y., Wirtz, D. & Hanes, J. Micro- and macrorheology of mucus. *Adv Drug Deliv Rev* **61**, 86-100, doi:10.1016/j.addr.2008.09.012 (2009).
- 11 Matsuo, K., Ota, H., Akamatsu, T., Sugiyama, A. & Katsuyama, T. Histochemistry of the surface mucous gel layer of the human colon. *Gut* **40**, 782-789, doi:10.1136/gut.40.6.782 (1997).
- 12 Jordan, N., Newton, J., Pearson, J. & Allen, A. A novel method for the visualization of the in situ mucus layer in rat and man. *Clin Sci (Lond)* **95**, 97-106 (1998).
- 13 Szentkuti, L. & Lorenz, K. The thickness of the mucus layer in different segments of the rat intestine. *Histochem J* **27**, 466-472 (1995).
- 14 Schroeder, B. O. Fight them or feed them: how the intestinal mucus layer manages the gut microbiota. *Gastroenterol Rep (Oxf)* **7**, 3-12, doi:10.1093/gastro/goy052 (2019).
- 15 Bhaskar, K. R. *et al.* Viscous fingering of HCl through gastric mucin. *Nature* **360**, 458-461, doi:10.1038/360458a0 (1992).
- 16 Janmey, P. A., Georges, P. C. & Hvidt, S. Basic rheology for biologists. *Methods Cell Biol* **83**, 3-27, doi:10.1016/S0091-679X(07)83001-9 (2007).

- 17 Ensign, L. M., Cone, R. & Hanes, J. Oral drug delivery with polymeric nanoparticles: the gastrointestinal mucus barriers. *Adv Drug Deliv Rev* **64**, 557-570, doi:10.1016/j.addr.2011.12.009 (2012).
- 18 Sellers, L. A., Allen, A., Morris, E. R. & Ross-Murphy, S. B. The rheology of pig small intestinal and colonic mucus: weakening of gel structure by non-mucin components. **1115**, 174-179 (1991).
- 19 Sellers, L. A., Allen, A., Morris, E. R. & Ross-Murphy, S. B. Mechanical characterization and properties of gastrointestinal mucus gel. *Biorheology* **24**, 615-623, doi:10.3233/bir-1987-24614 (1987).
- 20 Sardelli, L. *et al.* Towards bioinspired in vitro models of intestinal mucus. *RSC Advances* **9**, 15887-15899 (2019).
- 21 Bell, A. E. *et al.* Properties of Gastric and Duodenal Mucus: Effect of Proteolysis, Disulfide Reduction, Bile, Acid, Ethanol, and Hypertonicity on Mucus Gel Structure. *Gastroenterology* **88**, 269-280 (1985).
- 22 Macierzanka, A. *et al.* Transport of Particles in Intestinal Mucus under Simulated Infant and Adult Physiological Conditions: Impact of Mucus Structure and Extracellular DNA. *PLOS ONE* **9**, e95274 (2014).
- 23 Boegh, M., Baldursdóttir, S. G., Müllertz, A. & Nielsen, H. M. Property profiling of biosimilar mucus in a novel mucus-containing in vitro model for assessment of intestinal drug absorption. **87**, 227-235 (2014).

- 24 Meldrum, O. W. *et al.* Mucin gel assembly is controlled by a collective action of non-mucin proteins, disulfide bridges, Ca(2+)-mediated links, and hydrogen bonding. *Sci Rep* **8**, 5802, doi:10.1038/s41598-018-24223-3 (2018).
- 25 Macierzanka, A. *et al.* Adsorption of bile salts to particles allows penetration of intestinal mucus. *Soft Matter* **7**, 8077-8084 (2011).
- 26 Nordgård, C. T. & Draget, K. I. Dynamic responses in small intestinal mucus: Relevance for the maintenance of an intact barrier. *Biological Barriers* **95**, 144-150 (2015).
- 27 Piatigorski, B. *Fluid flow fields in the hydrodynamic attachment of Giardia lamblia to grooved substrates*, Georgetown University, (2018).
- 28 Picou, T. J. *The Hydrodynamic Model of Giardia lamblia Attachment* PhD thesis, Georgetown University, (2017).
- 29 Feely, D. E., Erlandsen, S. L. & Chase, D. G. 3-32 (Plenum Press, New York, 1984).
- 30 Luján, H. & Svärd, S. *Giardia: A Model Organism*. Chapter 9 (2011).
- 31 Rubinstein, M. & Colby, R. H. *Polymer Physics (Chemistry)*. Chapter 9 (Oxford University Press, 2003).
- 32 Axelsson, M. A. B., Asker, N. & Hansson, G. C. O-Glycosylated MUC2 Monomer and Dimer from LS 174T Cells Are Water-soluble, whereas Larger MUC2 Species Formed Early during Biosynthesis Are Insoluble and Contain Nonreducible Intermolecular Bonds. *Journal of Biological Chemistry* **273**, 18864-18870 (1998).
- 33 Almutairi, F. M. *et al.* Application of recent advances in hydrodynamic methods for characterising mucins in solution. **45**, 45-54 (2016).

- 34 Saleh, H. M., Annuar, M. S. M. & Simarani, K. Ultrasound degradation of xanthan polymer in aqueous solution: Its scission mechanism and the effect of NaCl incorporation. *Ultrasonics Sonochemistry* **39**, 250-261, doi:<https://doi.org/10.1016/j.ultsonch.2017.04.038> (2017).
- 35 Kurenkov, V. F., Hartan, H.-G. & Lobanov, F. I. Degradation of Polyacrylamide and Its Derivatives in Aqueous Solutions. *Russian Journal of Applied Chemistry* **75**, 1039-1050, doi:10.1023/a:1020747523268 (2002).
- 36 Vijayalakshmi, S. P. & Madras, G. Effect of temperature on the ultrasonic degradation of polyacrylamide and poly(ethylene oxide). *Polymer Degradation and Stability* **84**, 341-344, doi:<https://doi.org/10.1016/j.polymdegradstab.2004.02.007> (2004).
- 37 Mason, T. J. & Lorimer, J. P. pp. 39 (Wiley-VCH, 2002).
- 38 Camesano, T. A. & Wilkinson, K. J. Single molecule study of xanthan conformation using atomic force microscopy. *Biomacromolecules* **2**, 1184-1191, doi:10.1021/bm015555g (2001).
- 39 Chun, M.-S. & Park, O. O. On the intrinsic viscosity of anionic and nonionic rodlike polysaccharide solutions. *Macromolecular Chemistry and Physics* **195**, 701-711 (1994).
- 40 Keister, D. B. Axenic culture of *Giardia lamblia* in TYI-S-33 medium supplemented with bile. *Trans R Soc Trop Med Hyg* **77**, 487-488, doi:10.1016/0035-9203(83)90120-7 (1983).

- 41 Chen, P. *et al.* Experimental and theoretical study of dilute polyacrylamide solutions: effect of salt concentration. **18**, 3153-3160 (2012).
- 42 Matthews, L. W., Spector, S., Lemm, J. & Potter, J. L. Studies on Pulmonary Secretions. *American Review of Respiratory Disease* **88**, 199-204 (1963).
- 43 Potter, J. L., Matthews, L. W., Spector, S. & Lemm, J. Studies on Pulmonary Secretions. *American Review of Respiratory Disease* **96**, 83-87 (1967).
- 44 Crowther, R. S., Marriott, C. & James, S. L. Cation induced changes in the rheological properties of purified mucus glycoprotein gels. *Biorheology* **21**, 253-263, doi:10.3233/bir-1984-211-227 (1984).
- 45 Tagavifar, M. *Enhanced heavy oil recovery by hybrid thermal-chemical processes*, (2014).
- 46 Ball, J. T. & Pitts, M. J. Effect of Varying Polyacrylamide Molecular Weight on Tertiary Oil Recovery From Porous Media of Varying Permeability. *SPE Enhanced Oil Recovery Symposium*, 8 (1984).
- 47 Kulakov, L. A., McAlister, M. B., Ogden, K. L., Larkin, M. J. & O'Hanlon, J. F. Analysis of bacteria contaminating ultrapure water in industrial systems. *Applied and environmental microbiology* **68**, 1548-1555 (2002).
- 48 Xiong, B. *et al.* Polyacrylamide degradation and its implications in environmental systems. **1**, 17 (2018).
- 49 Teodorovic, S., Braverman, J. M. & Elmendorf, H. G. Unusually Low Levels of Genetic Variation among *Giardia lamblia* Isolates. *Eukaryotic Cell* **6**, 1421 (2007).

Supplemental Information

SI.1 Rheology and qualitative growth curves for Ficoll in media. Ficoll 400kDa (Sigma Life Sciences) was added to *Giardia* media to increase the viscosity of the solution. LCPAM changes both the viscosity and elasticity of a solution, but Ficoll changes the viscosity without significantly changing the elasticity. Thus, we could compare *Giardia* growth in LCPAM and Ficoll to determine if *Giardia* growth is sensitive to elasticity and viscosity, or only to viscosity. This experiment was executed, but due to difficulties of culturing *Giardia* in Ficoll, Ficoll was discontinued in this study. However, the rheological values for Ficoll in media are provided below.

In contrast to shear-thinning LCPAM solutions, 10%, 15%, 20%, and 24% Ficoll in media exhibit Newtonian behavior (Figure SI1a). Theoretically, Ficoll should not exhibit elastic behavior in oscillatory rheology measurements; with the assumption that $G' = 0$, the theoretical G'' is

$$G''(\omega) = \omega\eta \quad (S1)$$

where η is the viscosity of Ficoll (which, due to Newtonian behavior, does not change with shear rate). Although the oscillatory measurements of Ficoll report a non-zero value for G' , the theoretical G'' is approximately the same as the experimental G'' (compare dotted lines with triangles, Figure SI1b).

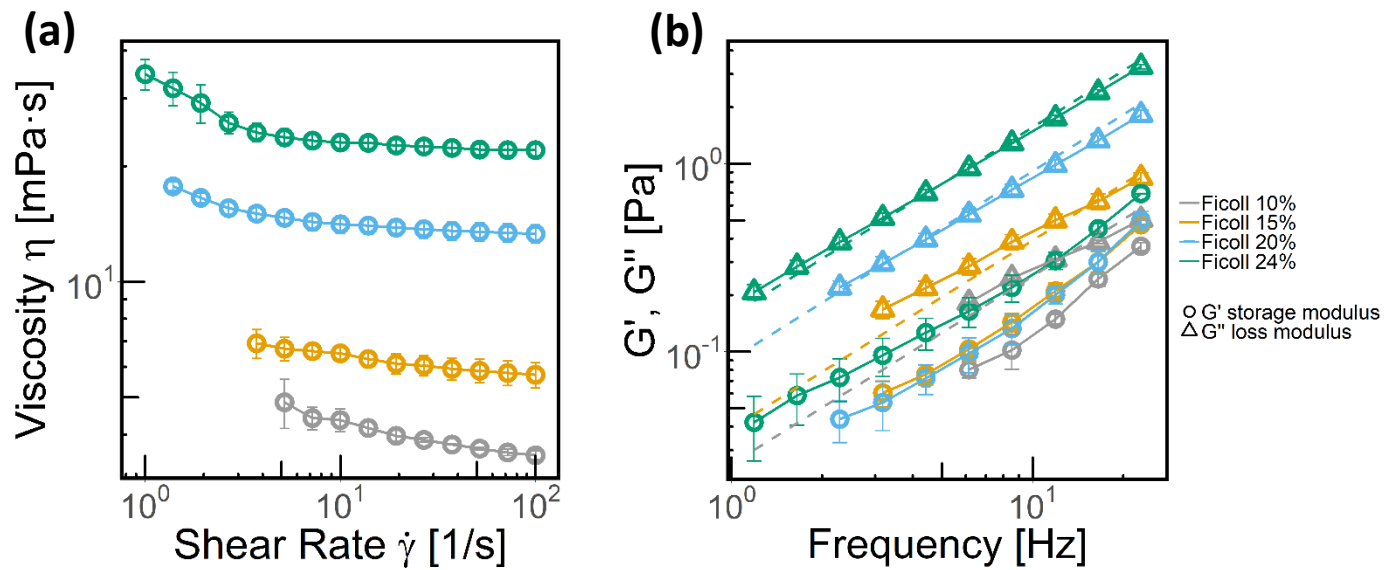


Figure S11. Flow curve **(a)** and frequency sweep **(b)** of 10% Ficoll (grey, $n = 2$), 15% Ficoll (orange, $n = 2$), 20% Ficoll (blue, $n = 2$), and 24% Ficoll (green, $n = 2$). Error bars show the standard deviation of samples. **(b)** Circles are the storage modulus (G'), triangles are the loss modulus (G''). The dotted line represents theoretical G'' calculation from equation S1.

Qualitative observations of *Giardia* growth suggest that growth behavior is approximately the same in 24% Ficoll and 0.4% LCPAM. These two solutions have approximately the same viscosity within the characteristic shear rate range for *Giardia* (compare purple with yellow within shear rate 10 - 100 s^{-1} , Figure S12). Thus, a quantitative growth curve assay was done with control media, 0.4% LCPAM, and 24% Ficoll. However, *Giardia*'s cell density for 24% Ficoll did not increase for 6.5 days. Additionally, tubes of *Giardia* in Ficoll were highly prone to contamination. Due to experimental difficulties, Ficoll was no longer used in *Giardia* growth experiments.

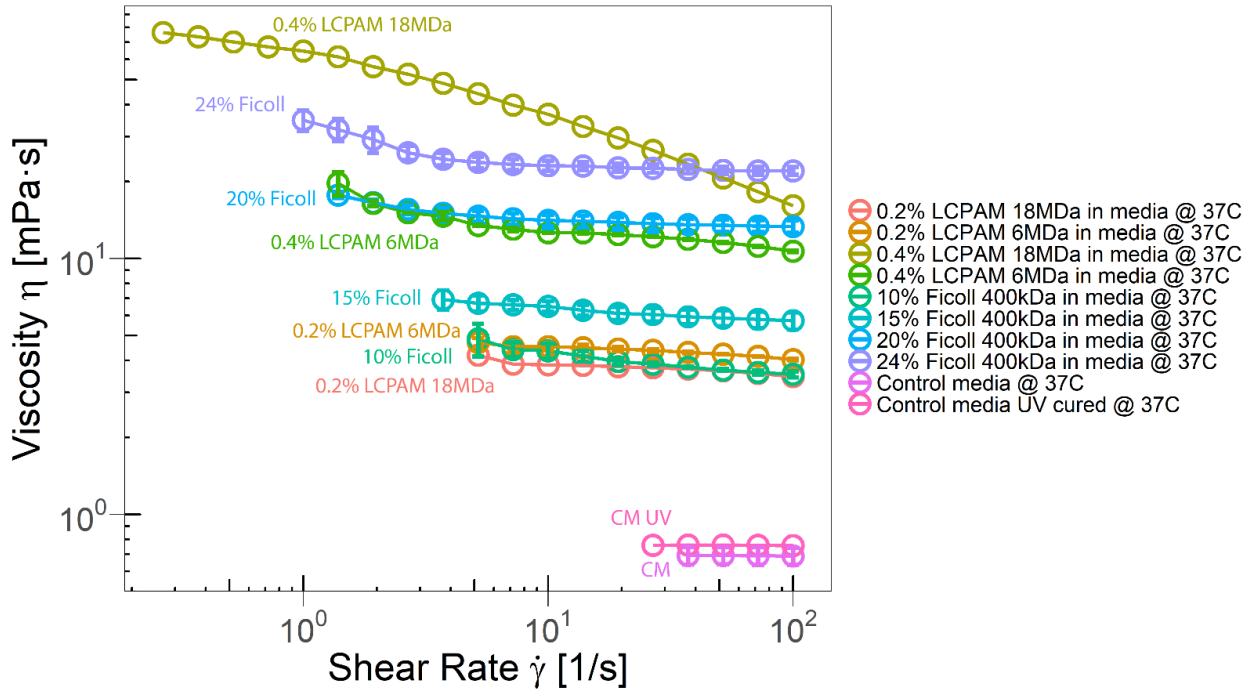


Figure SI2. Flow curve for all solutions of LCPAM, Ficoll, and control media. All rheological measurements were taken at 37°C.

SI.2 Image processing for automated *Giardia* counting.

Before counting *Giardia* cells manually under a light microscope, we attempted to automate the process through image processing. Cells were cultured in cell chamber slides, and growth was imaged over time. Unlike tubes, chamber slides have a flat bottom in which cells can be imaged with a confocal microscope. Images of the chambers were taken approximately every 12 or 24 hours (see Figure SI3a for an example).

A Python program was developed to identify living *Giardia* cells. The program was adapted from Trackpy, a Python package for particle tracking and image processing. The program was trained to correctly identify *Giardia* cells (bright features against a dark background) using a variety of parameters. Parameters that were effective in correctly identifying features include diameter, minimum mass (brightness), max size, separation

distance, and eccentricity. Parameters that did not significantly change feature identification include percentile minimum for peak brightness, threshold for bandpass, and smoothing size. All of these parameters are described on the Trackpy website (<http://soft-matter.github.io/trackpy/v0.4.2/>).

Trackpy is effective at counting *Giardia* cells when the image quality is good (Figure S13b). Images that are easier to process have a background that is blurred with even contrast, *Giardia* cells that do not overlap with each other, bright cells with a dark outline, and the absence of impurities such as black blobs (debris) or bright dead cell clumps. Unfortunately, these criteria were rarely met as it was difficult to obtain clean images. Additionally, cells cultured in chambers were highly prone to contamination, possibly due to the loose seal between the chamber and the glass slide. Imaging was difficult for chambers due to the presence of bubbles in the chamber, which interfered with the light from the microscope. Thus, Trackpy was discontinued for this experiment, and quantitative growth curves were executed by manual counting (see Section 3.4.4).

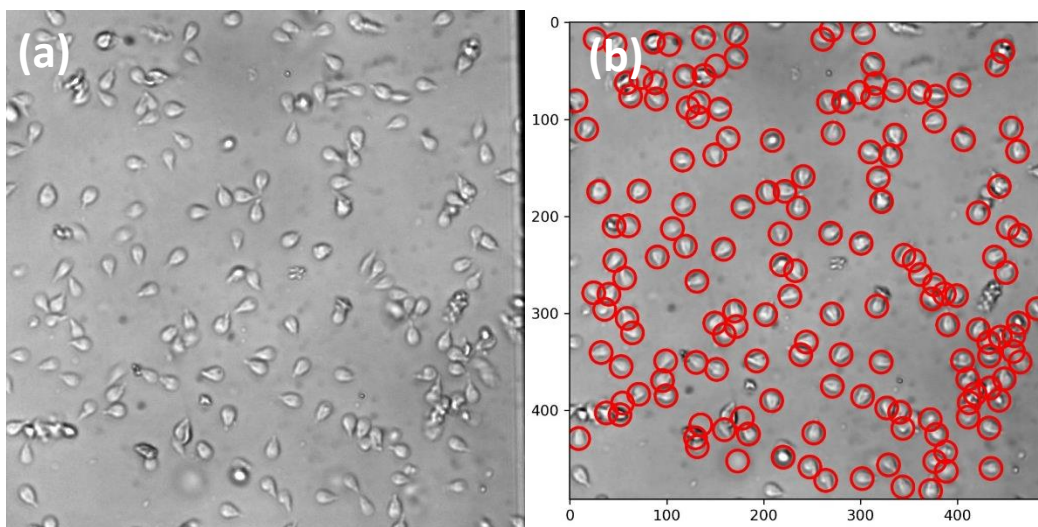


Figure S13. (a) Confocal image of chamber slide with *Giardia* grown in control media at 17 hours. (b) Using the Trackpy Python package, living *Giardia* cells were identified with red circles. Axes represent pixel dimensions.